33rd Annual International Conference of the IEEE EMBS
Boston, Massachusetts USA, August 30 - September 3, 2011

Compressed Sensing MRI Using Singular Value Decomposition Based Sparsity Basis

Yeyang Yu[1], Mingjian Hong[2], Feng Liu[1], Hua Wang[1], and Stuart Crozier[1], *Member, IEEE*

***Abstract*—Magnetic Resonance Imaging (MRI) is an essential medical imaging tool limited by the data acquisition speed. Compressed Sensing is a newly proposed technique applied in MRI for fast imaging with the prior knowledge that the signals are sparse in a special mathematic basis (called the 'sparsity' basis). During the exploitation of the sparsity in MR images, there are two kinds of 'sparsifying' transforms: predefined transforms and data adaptive transforms. Conventionally, predefined transforms, such as the discrete cosine transform and discrete wavelet transform, have been adopted in compressed sensing MRI. Because of their independence from the object images, the conventional transforms can only provide ideal sparse representations for limited types of MR images. To overcome this limitation, this work proposed Singular Value Decomposition as a data-adaptive sparsity basis for compressed sensing MRI that can potentially sparsify a broader range of MRI images. The proposed method was evaluated by a comparison with other commonly used predefined sparsifying transformations. The comparison shows that the proposed method could give a sparser representation for a broader range of MR images and could improve the image quality, thus providing a simple and effective alternative solution for the application of compressed sensing in MRI.**

I. Introduction

MAGNETIC Resonance Imaging (MRI) [1], a non-invasive medical imaging technique, is excellent for imaging soft tissue. Conventionally, the full *k*-space is sampled and then an inverse Fourier transform is performed to reconstruct the image. However, because of the physical and physiological limitations, the acquisition of the full *k*-space data is time-consuming. A promising method to speed up the data acquisition is by reducing the total amount of *k*-space measurements using the parallel MRI (pMRI) technique. The pMRI technique includes the SiMultaneous Acquisition of Spatial Harmonics (SMASH)[2], the Sensitivity Encoding for fast MRI (SENSE)[3], or the GeneRalized Autocalibrating Partially-Parallel Acquisitions (GRAPPA)[4]. However, due to the signal noise and the imperfect coil geometry, these techniques practically face a trade-off between image quality and speed.

Alternatively, Compressed Sensing (CS)[5] is a recently proposed technique applied in MRI to reduce the *k*-space measurements through the exploitation of sparsity in the MR images, therefore the application of CS in MRI (CS-MRI)[6][7] can potentially speed up the overall data acquisition process. In CS-MRI, there are two fundamental conditions, (i) a special mathematic basis (usually called 'sparsity' basis) is used for the sparse representation of the object image and, (ii) the sparsity basis should be incoherent with the sensing basis (the Fourier transform basis). With these two conditions, the object image can be accurately reconstructed with an appropriate nonlinear recovery algorithm. A pseudo-random variable density *k*-space under-sampling scheme is typically applied to ensure the incoherence between the sensing basis and the sparsity basis. To enforce the sparsity of the MR images, the conventional method is to project the images on to the predefined sparsifying transform bases, such as the discrete cosine transform basis[8] and the discrete wavelet transform basis[9]. These predefined bases can only provide an ideal sparse representation for limited types of object images.

To overcome the limitation of the conventional sparsity bases, this work proposes a new method using Singular Value Decomposition (SVD)[10] as a data-adaptive sparsifying transformation for CS-MRI. The proposed method was evaluated with the brain image and an angiogram, which represent diverse image features.

II. Methodology

A. Compressed Sensing in MRI (CS-MRI)

CS can be successfully applied to MRI based on the prior knowledge that the MR images can be sparsely represented in an appropriate basis (sparsity basis). Moreover, by applying the random under-sampling scheme in the *k*-space, the aliasing artifacts are incoherent in the sparsity basis. Therefore, the sparsity coefficients can be recovered by using an appropriate non-linear reconstruction algorithm, and as a consequence recovering the MR images. Mathematically, the CS-MRI framework can be formulated as the following constrained optimization problem:

$$\begin{aligned} &Minimize: \left\|\Psi(m)\right\|_1 \\ &s.t. \left\|\Phi_F(m) - y\right\|_2 < \varepsilon \end{aligned} \tag{1}$$

Where m is an $M \times M$ MR image, $\mathbf{\Psi}$ denotes the sparsifying transformation, $\mathbf{\Phi_F}$ denotes the partial Fourier

Manuscript received April 14, 2011. This work was supported in part by the Australian Research Council.

Yeyang Yu is with the School of Information Technology and Electrical Engineering (school of ITEE), the University of Queensland (UQ), Brisbane, Australia. (Email: yeyang.yu@uq.edu.au)

Mingjian Hong is with the School of Software Engineering, ChongQing University, Chongqing, China. (Email: mingjian.hong@uq.edu.au)

Feng Liu, and is with the school of ITEE, UQ, Brisbane, Australia. (Email: feng@itee.uq.edu.au)

Hua Wang is with the school of ITEE, UQ, Brisbane, Australia. (Email: hwang@itee.uq.edu.au)

Stuart Crozier is with the school of ITEE, UQ, Brisbane, Australia. (Email: stuart@itee.uq.edu.au).

transform, *y (y‹‹ M×M)* are the measurements collected from the MRI scanner and ε relates to the noise level of the measurements. The constrained convex optimization problem in equation (1) was solved as follows by considering its Lagrangian form described as:

$$\text{Minimize: } f(m) = \left\|\Phi_F(m) - y\right\|_2 - \lambda\left\|\Psi(m)\right\|_1 \qquad (2)$$

The non-linear conjugate gradient (NLCG) was applied to solve the unconstrained problem in the Lagrangian form, as described in equations (2). The algorithm was implemented in Matlab (Release 2010a). All simulations were performed on a MacBook Pro with a 2.4 GHz Intel Core 2 Duo processor and a 4 GB memory.

B. MRI Object Images

Fig. 1 shows a brain image and an angiogram that were used to test the reconstruction performance of the CS-MRI algorithms. Both images are fully sampled with a resolution of 512 by 512 pixels. The brain image was obtained in a Bruker 2T whole-body MRI system. The brain image is not naturally sparse in the pixel domain, so that it can be used to test the performance of the methods on general MRI images. The MRI angiogram was obtained in a Siemens MAGNETOM Avanto 1.5T system. The MRI angiogram can represent those special MR images already sparse in the pixel domain.

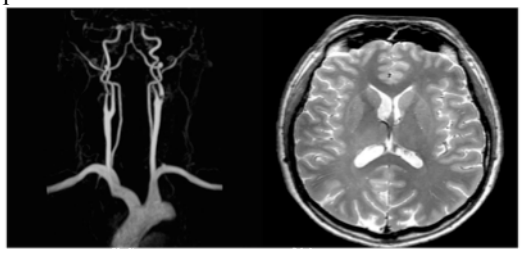

Fig. 1. The original angiogram and brain image.

Both images were evaluated from three aspects, (i) the peak SNR (PSNR) and the gray scale value of $\|\phi_F(m) - y\|_2$ to test the quality of the image, (ii) the image reconstruction time to test the computing efficiency and, iii) the gray scale values of $\|\Psi(m)\|_1$ for sparsity. The PSNR is calculated by:

$$PSNR = 10\log_{10}\frac{1}{MSE} \qquad (3)$$

Where the MSE is the mean squared error between the original and the reconstructed images.

C. K-space sampling scheme

In CS the *k*-space was under-sampled to reduce the measurements need, and as a result to shorten the scan time. In this work, the *k*-space was randomly under-sampled along the phase direction with a Gaussian density distribution. The central region of the *k*-space was fully sampled because it contains the major low frequency information. By adjusting the density function, 110 lines, 140 lines, 170 lines, 200 lines, 230 lines, and 260 lines were randomly chosen from the full k-space data respectively.

D. Using SVD to Construct The Data-adaptive Sparsifying Transform Ψ

1) Constructing the initial estimate of the sparsifying transformation Ψ

Based on the under-sampled *k*-space data, the image ($\boldsymbol{I_{zf}}$) was reconstructed by an inverse Fourier transform. Because the centre of the *k*-space was fully sampled, the dominant information of the desired image *M* was therefore kept, the image $\boldsymbol{I_{zf}}$ should be a good initial estimate for *M*.

As it is shown in the top row of Fig. 2, for image $\boldsymbol{I_{zf}}$, its SVD can be expressed as

$$\boldsymbol{I_{zf}} = \boldsymbol{U_0}\boldsymbol{\Sigma_{zf}}\boldsymbol{V_0}^* \qquad (4)$$

The initial estimate of the sparsifying transform can be written as follows.

$$\boldsymbol{\Psi_0}(m) = \boldsymbol{U_0}^* m \boldsymbol{V_0} \qquad (5)$$

To test whether U_0 and V_0 are able to give a sparse representation for the desired image *M,* we projected *M* onto U_0 and V_0, and the result is shown in the bottom row of Fig. 2.

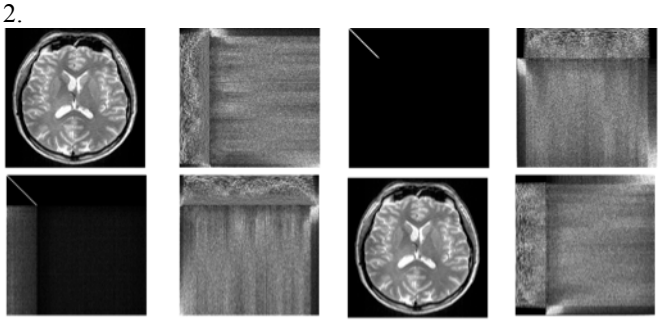

The top shows the process of generating the sparsity basis, from left to right: the image $\boldsymbol{I_{zf}}$, the unitary matrix $\boldsymbol{U_0}$, the diagonal matrix $\boldsymbol{\Sigma_{zf}}$, and the unitary matrix $\boldsymbol{V_0}^*$; the bottom raw shows the test of the sparse representation of the desired image, from left to right: the sparse representation of the desired image M, the unitary matrix $\boldsymbol{U_0}^*$, the desired image $\boldsymbol{M}$, and the unitary matrix $\boldsymbol{V_0}$.

2) Updating the sparsifty basis Ψ

With the $\boldsymbol{\Psi_0}(m)$ from equation (5), we can use NLCG to solve the problem in equation (2) and obtain the first reconstrcted image M_1. However, M_1 is not the optimal estimate because the U_0 and V_0 in equation (5) are sub-optimal estimates of the sparsifying transform for the desired image *M*. To seek a better estimate, we update the matrices *U* and *V* iteratively by performing SVD on the reconstruction result of equation (2) M_1 as a new prior image data, and repeat this until the image quality of the k^{th} reconstructed image M_k get stable. According to our prior observation, M_k got stable after 2 or 3 times iteration.

III. Results

A. The Brain Image

The discrete wavelet transform (DWT) and the discrete cosine transform (DCT), as the conventionally used sparsity bases in the brain image case, were implemented to compare with the proposed method. Fig. 3 and TABLE I to IV show that the proposed method is faster in computation, achieves better image quality, and represents the image sparser.

1) Faster in computing time

TABLE I shows that the SVD-based method outperformed the DWT and DCT-based method in computing time. Especially compared to the DWT-based method, the proposed was near twice faster.

2) Better image quality

Fig. 3 is the brain reconstruction result with 140 sampling lines of the *k*-space. Fig 3 shows that the three methods achieved very close image quality. TABLE II illustrates the comparison of the PSNR achieved by the SVD-, DWT-, and DCT-based methods. Higher PSNR value stands for better image quality. With different *k*-space lines sampled, the proposed method achieved the highest PSNR value among

TABLE I
COMPARISON OF COMPUTING TIME (S) OF DIFFERENT SPARSIFYING BASES FOR DIFFERENT KINDS OF MRI IMAGES.

NO. of *k-space* lines sampled	110	140	170	200	230	260
Brain						
SVD	161.5	158.8	171.7	167.5	172.9	156.9
DWT	300.8	301.9	299.9	302.3	306.6	303.5
DCT	216.4	217.2	216.9	220.8	225.7	221.4
Angiogram						
SVD	152.4	159.4	164.9	156.1	154.4	192.7
DWT	305.1	318.3	309.2	392.6	304.3	306.3
IDT	52.2	59.0	56.4	51.7	57.5	53.6

the others. Averagely, the SVD basis provided 0.57 (db) higher PSNR value than the DWT-based method, and 1.03 (db) higher PSNR value than the DCT-based method. In TABLE III, the gray scale values of $\|\boldsymbol{\phi}_F(m) - y\|_2$ achieved by the three methods were compared. Smaller gray scale values of $\|\boldsymbol{\phi}_F(m) - y\|_2$ indicate better data fidelity. Table III shows that the proposed method provided the smallest l_2 norm value at each *k*-space sampling rate. In average, the l_2 norm value of $\|\boldsymbol{\phi}_F(m) - y\|_2$ achieved by the propose method was 2.97 smaller than the DWT-based method, and 2.65 smaller than the DCT-based method. These demonstrate that the proposed method offered better image quality.

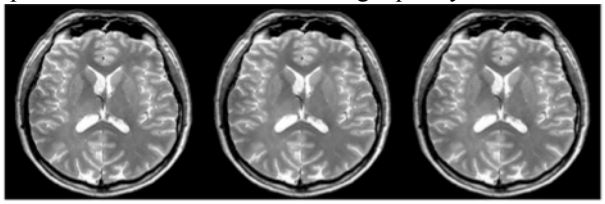

Fig. 3. The results of the brain image reconstruction with 140 lines sampled, from left to right the sparsifying transforms applied are: SVD, DWT, and DCT.

TABLE II
COMPARISON OF THE IMAGE QUALITY IN TERMS OF PSNR (db)

NO. of k-space lines sampled	110	140	170	200	230	260
Brain						
SVD	25.82	27.73	29.60	31.49	32.94	35.12
DWT	25.55	27.28	29.18	30.97	32.32	33.96
DCT	25.02	27.10	28.90	30.45	31.67	33.35
Angiogram						
SVD	37.90	41.47	44.88	48.38	50.37	51.96
DWT	37.26	39.42	41.36	42.89	43.75	44.48
IDT	35.49	35.93	36.21	36.34	36.38	36.41

TABLE III
COMPARISON OF THE DATA FIDELITY IN TERMS OF l_2 NORM $\|\phi_F(m) - y\|_2$

NO. of k-space lines sampled	110	140	170	200	230	260
Brain						
SVD	1.32	1.33	1.47	1.49	1.58	1.38
DWT	4.22	4.25	4.30	4.38	4.59	4.70
DCT	3.48	3.66	3.95	4.20	4.50	4.68
Angiogram						
SVD	0.64	0.62	0.66	0.64	0.67	0.71
DWT	2.28	2.25	2.35	2.40	2.42	2.47
IDT	7.66	7.66	7.68	7.69	7.69	7.69

3) Sparser representation

The gray scale values of $\|\boldsymbol{\Psi}(m)\|_1$ achieved by the three methods were presented in TABLE IV. Smaller l_1 norm value stands for sparser representation. With different lines of *k*-space sampled, the SVD-based method provided the smallest gray scale values of $\|\boldsymbol{\psi}(m)\|_1$, and averagely it provided 8201.50 smaller gray scale values of $\|\boldsymbol{\psi}(m)\|_1$ than the DWT-based method, and 7691.50 smaller than the DCT-based method. These illustrate that the SVD transform provided a sparser representation for the brain image, which represents the general MR images.

TABLE IV
COMPARISON OF THE SPARSITY IN TERMS OF l_1 NORM $\|\psi(m)\|_1$

NO. of k-space lines sampled	110	140	170	200	230	260
Brain						
SVD	793.76	832.74	868.82	894.79	914.46	929.10
DWT	8107.05	8529.20	9029.12	9394.12	9592.65	9788.10
DCT	7057.33	7831.90	8475.66	8985.24	9342.80	9689.67
Angiogram						
SVD	323.47	336.09	330.30	334.42	356.14	350.10
DWT	2507.36	2599.40	2627.37	2663.42	2682.91	2696.19

IDT	14062.74	14061.69	14050.92	14048.13	14047.60	14048.69

B. The Angiogram

The angiogram is naturally sparse in the image domain, so the identity transform (IDT) is used for these types of images for the sparsity basis. The IDT, DWT and SVD bases were applied in this case to compare the reconstruction performances. Fig. 4 and TABLE I to IVThe proposed method out-performed IDT and DWT on image quality and sparse representation.

1) Medium computation speed

In TABLE I, the SVD-based method was slower (roughly three times) in computation than the IDT-based method at each k-space sampling rate. But it was still faster than the DWT-based method. And the computing time of the SVD method was averagely 50.52% of that of the DWT-based method.

2) Better image quality

Fig. 4 is the angiogram reconstruction result with 140 lines of the *k*-space sampled. In Fig. 4, the image qualities from the three methods were quite close to each other. In TABLE II the PSNR of the proposed method was slightly higher than the other methods at the six different sampling rates. In average, the SVD-based method provided 4.30 (db) higher PSNR value than the DWT-based method, and 9.70 (db) higher than the IDT-based method. In TABLE III, the data fidelity was compared and the proposed method achieved the best data fidelity. Averagely the gray scale values of $\|\boldsymbol{\phi}_F(m) - y\|_2$ in the SVD-based method was 1.71 smaller than the DWT-based method, and was 7.02 smaller than the IDT-based method. The results showed in TABLE II and TABLE III demonstrate that the proposed method achieved better image quality.

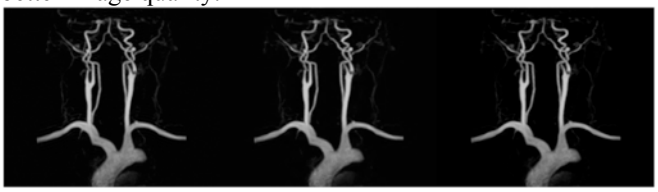

Fig. 4. The results of the angiogram reconstruction with 140 lines sampled, from left to right the sparsifying transforms applied are: SVD, DWT, and IDT.

3) Sparser representation

TABLE IV shows that at each *k*-space sampling rate, the gray scale values of $\|\boldsymbol{\psi}(m)\|_1$ in SVD basis were smaller than those in the DWT or IDT bases. In average, the gray scale values of $\|\boldsymbol{\psi}(m)\|_1$ in SVD basis was 2290.81 smaller than that in DWT basis, and was 1371.43 smaller than that in IDT basis. TABLE IV demonstrates that the proposed method was able to provide a sparser representation than the DWT and IDT bases.

IV. CONCLUSION

In this work, we developed and tested a Single Value Decomposition based data-adaptive sparsity basis for CS-MRI. From the case studies, it is found that compared with conventional bases, the proposed sparsity basis was able to provide a sparser representation for both types of MR images, recover image more accurately, thus improve the image quality in the CS-MRI applications. In the future work, this technique will be applied to dynamic MRI studies, where more prior image data is available for training data-adaptive sparsity basis.

REFERENCES

[1] C. Westbrook, C. K. Roth, and J. Talbot, *MRI in practice*. Wiley-Blackwell, 2005.

[2] D. Sodickson and W. Manning, "Simultaneous acquisition of spatial harmonics (SMASH): Fast imaging with radiofrequency coil arrays," *Magnetic Resonance in Medicine*, vol. 38, no. 4, pp. 591-603, Oct. 1997.

[3] K. P. Pruessmann, M. Weiger, M. B. Scheidegger, and P. Boesiger, "SENSE: sensitivity encoding for fast MRI," *Magnetic Resonance in Medicine*, vol. 42, no. 5, p. 952–962, 1999.

[4] M. A. Griswold et al., "Generalized autocalibrating partially parallel acquisitions (GRAPPA)," *Magnetic Resonance in Medicine*, vol. 47, no. 6, pp. 1202-1210, 2002.

[5] D. L. Donoho, "Compressed sensing," *Information Theory, IEEE Transactions on*, vol. 52, no. 4, pp. 1289-1306, 2006.

[6] M. Lustig, D. L. Donoho, J. M. Santos, and J. M. Pauly, "Compressed sensing MRI," *IEEE Signal Processing Magazine*, vol. 25, no. 2, p. 72–82, 2008.

[7] M. Lustig, D. Donoho, and J. M. Pauly, "Sparse MRI: The application of compressed sensing for rapid MR imaging," *Magnetic Resonance in Medicine*, vol. 58, no. 6, p. 1182–1195, 2007.

[8] S. A. Khayam, "The discrete cosine transform (dct): Theory and application," *Michigan State University*, 2003.

[9] S. G. Mallat, *A wavelet tour of signal processing*. Academic Press, 1999.

[10] N. Muller, L. Magaia, and B. M. Herbst, "Singular Value Decomposition, Eigenfaces, and 3D Reconstructions," *SIAM Review*, vol. 46, no. 3, p. 518, 2004.